4f levels of rare-earth hexaborides: A simple approach based on a modified orthogonalized-plane-wave method and a self-consistent-field atomic-structure calculation

Michihide Kitamura

Department of Electrical and Electronic Engineering, Faculty of Engineering, Utsunomiya University, Utsunomiya 321, Japan

(Received 18 June 1993; revised manuscript received 13 September 1993)

The electronic structures of trivalent and divalent rare-earth hexaborides RB_6 are calculated by using the modified orthogonalized-plane-wave method within the framework of the muffin-tin-potential approximation based on the self-consistent-field atomic-structure calculations. By regarding the $4f$ state as a partially filled corelike state and for the transition between $4f$ and $5d$ states, and adopting the transition state introduced by Slater which includes the effect of the screening of $4f$ states by $5d$ electrons, an attempt is made to understand the x-ray-photoemission spectroscopy (XPS) experiments and bremsstrahlung isochromat spectra (BIS). It is shown that the calculated results of the $4f$ levels relative to the Fermi level generally agree with the experimental ones obtained from the XPS for CeB_6, PrB_6, NdB_6, SmB_6, GdB_6, and YbB_6 and the BIS for GdB_6, TbB_6, and DyB_6, but there is a considerable difference between the calculations and experiments for the XPS for TbB_6, DyB_6, and HoB_6 and the BIS for LaB_6, CeB_6, and PrB_6. The reason for this disagreement is mainly attributed to the effect of $4f$ multiplets which is not taken into account in the present study.

I. INTRODUCTION

Rare-earth and actinide compounds known as "heavy fermion systems," show many interesting properties, e.g., valence fluctuation in SmB_6 (Ref. 1), abnormal magnetic resistivity in CeB_6 due to the dense Kondo effect,[2] a large electronic specific heat and an indication of superconductivity in Ce and U compounds,[3] etc. These properties come from the fact that these compounds all consist of elements having f electrons. Energy-band-structure calculations provide a powerful tool to study the electronic structure of matter. For rare-earth metals, approximate calculations of the band structures have been carried out[4–6] and the $4f$ binding energies estimated from x-ray photoemission spectroscopy (XPS) have been understood on the basis of the assumption that the photoexcited $4f$ states are completely screened by $5d$ electrons. For LaB_6, several band-structure calculations have been carried out,[7–10] and have shown that the calculated Fermi surface is consistent with de Haas–van Alphen measurements. However, there are few band-structure calculations for the rare-earth compounds having a finite number of $4f$ electrons because of the difficulty which arises when $4f$ electrons are regarded as valence electrons, and the complicated magnetic structure. Recently, band structure calculations based on the linearized muffin-tin-orbital (LMTO) (Ref. 11) and the Korringa-Kohn-Rostoker (KKR) (Ref. 12) methods have been performed for NdB_6, in which the $4f$ states have been regarded as partially filled corelike states, and which have explained well the experiment of the de Haas–van Alphen effect.

In the present paper, we calculate band structures of rare-earth hexaborides RB_6 (R = La, Ce, Pr, Nd, Sm, Eu, Gd, Tb, Dy, Ho, Er, Tm, Yb, and Lu) by using the modified orthogonalized-plane-wave (MOPW) method within the framework of the muffin-tin (MT) potential approximation based on the self-consistent-field (SCF) atomic-structure calculations. Using the results of the MOPW band-structure calculations, we determine the energy position of the $4f$ state relative to the Fermi level from the SCF atomic-structure calculations for rare-earth metal elements. The MOPW band-structure and SCF atomic-structure calculations, of course, need no empirical data. The aim of this paper is to estimate systematically the energy positions of $4f$ states relative to the Fermi level E_F, by joining the SCF atomic-structure calculations to the MOPW band-structure calculations in which $4f$ states are regarded as partially filled corelike states, and to compare these calculated results with both x-ray photoemission spectroscopy (XPS) (Refs. 13 and 14) and bremsstrahlung isochromat spectra (BIS).[14] XPS and BIS provide information about the $4f$ level, ε_{4f}, measured from the Fermi level E_F. We use the value of the Fermi level E_F obtained from MOPW band-structure calculation, to calculate the values of $\varepsilon^{(R)}_{4f(\mathrm{XPS})}$-$E_F$ and $\varepsilon^{(R)}_{4f(\mathrm{BIS})}$-$E_F$, which can be compared with experimental results of XPS and BIS. Our interest lies in checking to what extent our simple approach can explain the experimental results. The energy values of the $4f$ levels, $\varepsilon^{(R)}_{4f(\mathrm{XPS})}$ and $\varepsilon^{(R)}_{4f(\mathrm{BIS})}$, under the experimental situations of XPS and BIS, are calculated on the basis of the concept of the transition state introduced by Slater,[15] assuming that an electron-ejected rare-earth metal in the excitation process in the XPS, or an electron-accepted rare-earth metal in the recombination process in the BIS, can be treated as a single impurity atom embedded in crystals. In the present paper, we do not discuss the broadening of the spectra of XPS and BIS originating from the multiple structures of f states, which should be discussed as a many-electron problem based on solid-state physics.[13]

II. CALCULATION

Input data for the calculations are Herman and Skillman's atomic data[16] and the lattice constants.[17]

Starting from the self-consistent-field (SCF) atomic-structure calculations based on the prescription of Herman and Skillman, we obtain the atomic orbitals which are used to calculate the energy-band structures.

A. Band-structure calculation

Rare-earth hexaborides RB_6 belong to a simple cubic CaB_6-type structure and crystallize in a CsCl one in which Cs and Cl sites are replaced by R and octahedron B_6, respectively. Therefore, the corresponding first Brillouin zone (BZ) is also a simple cubic. The band-structure calculations are carried out by using the modified orthogonalized-plane-wave (MOPW) method. This method was developed by Deegan and Twose,[18] in order to avoid a difficulty which arises in the OPW method:[19] a slow convergence for the d-like conduction state. The reliability of the MOPW method has been checked by Farberovich and co-workers,[20–22] who performed band-structure calculations of the transition metals Nb and V (Ref. 20), semiconductors ZnS and CdS (Ref. 21), and rare-earth element Eu and its compounds EuO (Ref. 22), and compared these results with results obtained from the augmented-plane-wave (APW) method. Theoretical details for the MOPW method are given in Appendix A.

The muffin-tin (MT) radii $R_{\rm MT}$ are determined in such a way that the MT sphere for the R contacts along $\langle 100 \rangle$ directions, i.e., $R_{\rm MT}^{(R)}=a_0/2$, and that for the B contacts to the spheres of five nearest-neighbor B atoms, i.e., $R_{\rm MT}^{(\rm B)}=(\sqrt{2}-1)(a_0/2)$. The value of the Wigner-Seitz (WS) sphere $R_{\rm WS}$ is determined by the method we used to calculate the MT parameters of NaCl-, CsCl-, and CaF_2-type crystals.[23] In this method, it is assumed that the radius of the WS spheres is proportional to that of their MT ones. By using this method, we obtain the $R_{\rm WS}$ for R and B to be $\kappa R_{\rm MT}^{(R)}$ and $\kappa R_{\rm MT}^{(\rm B)}$. Here, κ is the proportional constant given by $a_0/\{\Omega_{\rm MT}^{(R)}+6\Omega_{\rm MT}^{(\rm B)}\}^{1/3}$, where $\Omega_{\rm MT}=4\pi R_{\rm MT}^3/3$. By using $V_0^{(R)}$ and $V_0^{(\rm B)}$, which are values obtained from the averaging of the crystal potential on the R and B sites in the region between the $R_{\rm MT}$ and $R_{\rm WS}$, the MT zero $V_{\rm MTZ}$ is calculated as $\{V_0^{(R)}+6V_0^{(\rm B)}\}/7$.

In the study of rare-earth compounds, the ionicity of the rare-earth elements plays an essential role in understanding the properties of the compounds. Therefore, the ionicity of the rare-earth elements, i.e., the effect of charge transfer, must be taken into account as exactly as possible. This is also true for the band-structure calculations of rare-earth hexaborides RB_6. We have calculated the Madelung energy, which is given by the third term of the right-hand side of Eq. (B7b), by using Evjen's method.[24] The Madelung energy is given by $(2/a_0)\sigma_\mu$, and the values of σ_μ are 3.107 495 for $\mu=R^{+3}$ and $-2.998\,661$ for $\mu=B^{-0.5}$ in atomic units. Here, it is noted that the value of σ_μ is reduced to $2\sigma_\mu/3$ for divalent rare-earth hexaborides $R^{+2}B_6^{-1/3}$.

Before doing the MOPW band-structure calculations of many rare-earth hexaborides, we have checked the convergence of the calculations for reciprocal-lattice vectors $\mathbf{G}$ defined by $(2\pi/a_0)(l,m,n)$ with integers l, m, and n. As a result, we have found that the calculation using a reciprocal lattice of 81 vectors is enough to obtain the converged result. In this case, the absolute value of the maximum reciprocal-lattice vector is $(2\pi/a_0)\sqrt{6}$. In the MOPW band-structure calculations, as can be seen from Eq. (A2a), Bloch states constructed from valence orbitals are added as basis states of the wave function. We use a $4f$ orbital as an additional basis state, so that the size of the matrix treated in the calculation is 88 ($=81+7$).

B. SCF atomic-structure calculation

In the XPS experiment for rare-earth compounds, a $4f$ electron is excited to continuum states by the radiation of an x ray. In a sample the condition of charge neutrality always must be satisfied, so that a vacancy due to the ejection of a $4f$ electron rapidly captures a d-like electron which obeys the dipole selection rule for the optical transition. In order to take into account these transition processes as exactly as possible, we adopt the concept of the transition state introduced by Slater. According to Slater's transition state for a $4f \rightarrow 5d$ transition, the electron configuration is given by $\mathrm{Xe}+4f^{n-0.5}5d^{0.5}6s^0$ ($1 \le n \le 14$). Here it is noted that there is no change of the ionicity of the photoexcited metal R^*. Using these electron configurations, we calculate the energy level of the photoexcited $4f$ state ($\varepsilon_{4f(\rm XPS)}^{(R)}$) on the basis of the SCF atomic-structure calculation.

BIS is, roughly speaking, the inverse process of XPS, i.e., electrons are injected from the external electron flow to a sample. The Slater transition state to be considered for an electron which drops into the $4f$ state is the transition from $5d$ to $4f$. Therefore, the electron configuration $\mathrm{Xe}+4f^n5d^16s^0$ for the initial state of the BIS is changed to $\mathrm{Xe}+4f^{n+0.5}5d^{0.5}6s^0$, where $0 \le n \le 13$. Using these electron configurations, the energy level of the $4f$ state ($\varepsilon_{4f(\rm BIS)}^{(R)}$) is obtained. In the BIS experiments for RB_6's, except for YbB_6 and LuB_6, it should be emphasized that the ionicity of an electron accepted-metal R^*, which is also treated as a single impurity as in the case of XPS, decreases by 1: contrary to the case for XPS.

The atomic orbitals used to carry out MOPW band-structure calculations are obtained from the SCF atomic-structure calculations in the following electron configurations: $\mathrm{Xe}+4f^n5d^06s^0$, where $n=0$, 1, 2, 3, 5, 7, 8, 9, 10, 11, 12, and 14 for trivalent La, Ce, Pr, Nd, Sm, Gd, Tb, Dy, Ho, Er, Tm, and Lu, and $n=6$, 7, and 14 for divalent Sm, Eu, and Yb, and are $1s^22s^22p^{1.5}$ for $B^{-0.5}$ and $1s^22s^22p^{4/3}$ for $B^{-1/3}$.

III. RESULTS AND DISCUSSION

We have calculated the energy-band structures of trivalent rare-earth hexaborides $R^{+3}B_6^{-0.5}$ (R=La, Ce, Pr, Nd, Sm, Gd, Tb, Dy, Ho, Er, Tm, and Lu) and of divalent ones $R^{+2}B_6^{-1/3}$ (R=Sm, Eu, and Yb) and obtained the densities of states. The densities of states were obtained from the sampling points of 4096 numbers defined within the first Brillouin zone Ω, where in practical calculations these sampling points are reduced to 165 points defined within the minimum segment given by

$\Omega/48$. The densities of states calculated for divalent and trivalent RB_6 are, of course, different from each other as shown in Figs. 1(a) and 1(b), in which the densities of states calculated for the divalent and trivalent SmB_6 are shown. We should emphasize that the densities of states calculated for different RB_6's with the same valency are almost the same, except that pointed density of states due to the $4f$ state of rare-earth elements appears at a different position. Some of the calculated densities of states are also shown in Figs. 1(c)–1(f): trivalent La and Ce hexaborides in Figs. 1(c) and 1(d), and divalent Eu and Yb ones in Figs. 1(e) and 1(f).

A. Comparison with XPS

Now let us compare the calculated densities of states with the experiments of x-ray photoemission spectroscopy (XPS).[13,14] Here the reader should remember that the

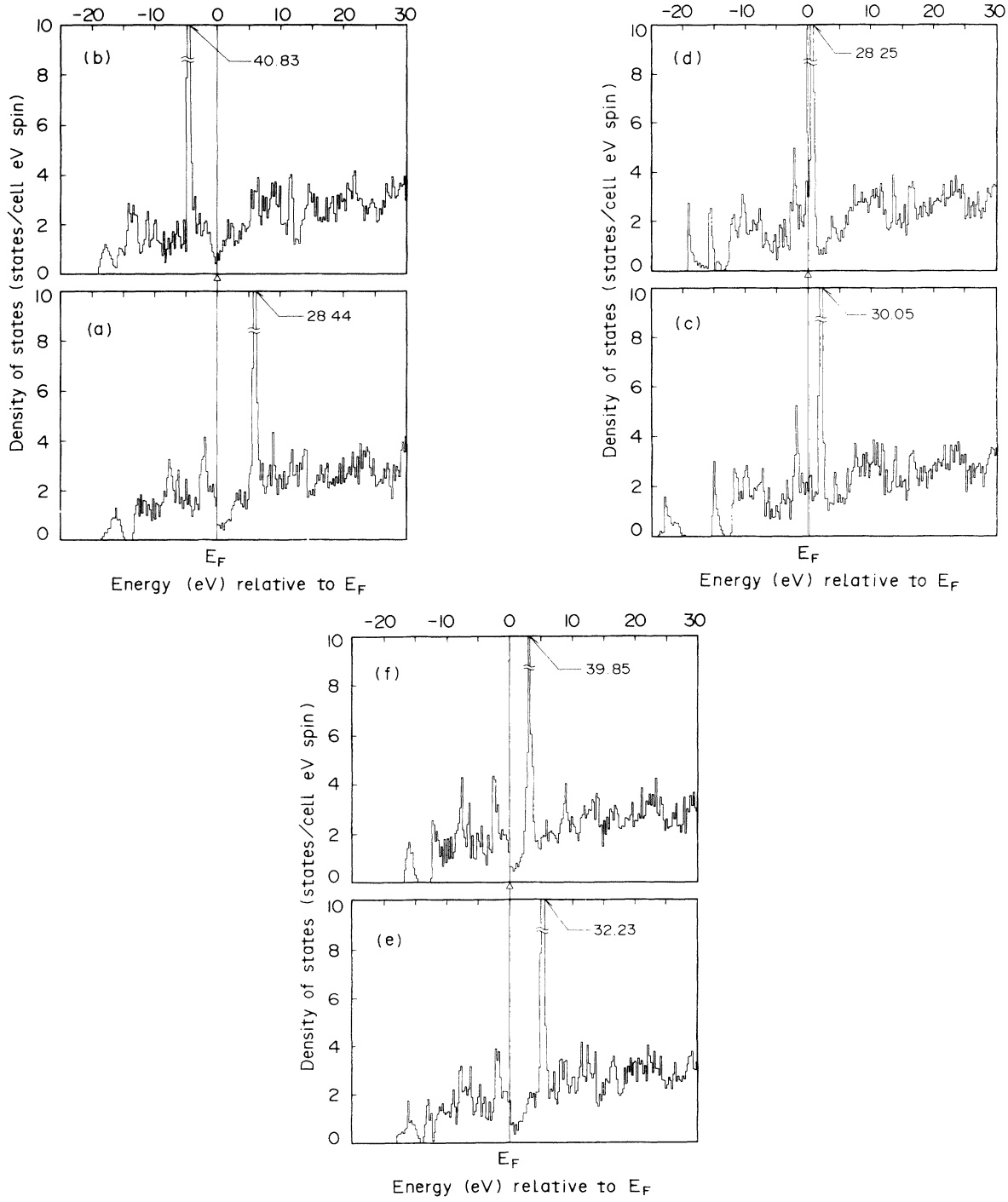

FIG. 1. Total densities of states (TDOS) calculated by the modified orthogonalized-plane-wave (MOPW) method: (a) divalent SmB_6, (b) trivalent SmB_6, (c) trivalent LaB_6, (d) trivalent CeB_6, (e) divalent EuB_6, and (f) divalent YbB_6. The energy is measured in units of eV from the Fermi level E_F indicated by the vertical line.

calculated densities of states are almost the same for the same valencies, except for the position of the energy level of the $4f$ state. The calculated results indicate explicitly that the difference between the XPS spectra for LaB_6 with no $4f$ electron and another RB_6 having a finite number of $4f$ electrons comes from the existence of $4f$ states occupied by a finite number of electrons. The positions of $4f$ states relative to the Fermi level E_F were obtained from the XPS spectra, by considering that for PrB_6 (Ref. 14), NdB_6 (Ref. 13), GdB_6 (Refs. 13 and 14), and YbB_6 (Ref. 14), the main peak corresponds to the energy position of $4f$ states, and that for SmB_6 (Ref. 13), TbB_6 (Refs. 13 and 14), DyB_6 (Ref. 14), and HoB_6 (Ref. 13), all the peaks correspond to the energy positions of $4f$ states, because there are considerable energy splittings due to $4f$ multiplets for the latter group. These are tabulated in Table I together with the values of ε_{4f}-E_F calculated for trivalent RB_6 (R = La, Ce, Pr, Nd, Sm, Gd, Tb, Dy, Ho, Er, Tm, and Lu) and divalent RB_6 (R = Sm, Eu, and Yb),

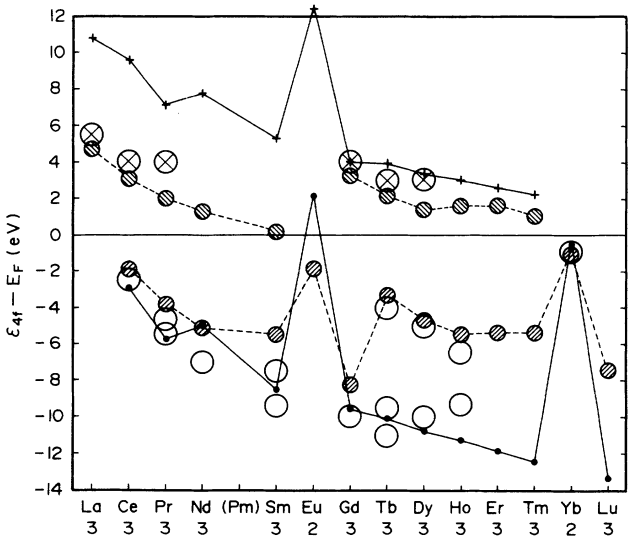

FIG. 2. Plot of the energy position of the $4f$ level ε_{4f} measured in units of eV from the Fermi level E_F as a function of rare-earth hexaborides RB_6 (R = La, Ce, Pr, Nd, Sm, Eu, Gd, Tb, Dy, Ho, Er, Tm, Yb, and Lu). The valencies used in the MOPW band-structure calculations for the RB_6's are also shown at the bottom of the figure. The calculated values of ε_{4f}-E_F's indicated by symbols ● and + are compared, respectively, with the experimental values (denoted by ○ and ⊗) obtained from the experiments with x-ray photoemission spectroscopy (XPS) and bremsstrahlung isochromat spectra (BIS). The Fermi level E_F was obtained from the MOPW band-structure calculation, and the value of ε_{4f} was calculated by using Eq. (C2c) consisting of the atomic energy term, the Madelung energy term, and the shift of the energy due to the crystallization. In the SCF atomic-structure calculation, Slater's transition state was adopted in order to describe the experimental situations of XPS and BIS. For comparison, the values of ε_{4f}-E_F for rare-earth metals calculated by Herbst, Watson, and Wilkins (Refs. 5 and 6) are also shown. The values indicated by symbols ○ and ○ correspond to XPS and BIS. Their calculation includes the effect of the Hund's rule $4f^{n-1}$ and $4f^{n+1}$ ground levels which correspond to XPS and BIS, respectively.

and the positions of the $4f$ states obtained from the experiments of ultraviolet photoemission spectroscopy (UPS) for CeB_6 and PrB_6 (Ref. 25).

The values of ε_{4f}-E_F obtained by using the electron configuration $4f^n5d^06s^0$ ($0 \le n \le 14$) for the ground states adopted in the MOPW band-structure calculations do not predict those obtained from the experiments; for example, in GdB_6 the calculated value is -5.89 eV, and the experimental one is -10.0 eV (see Table I). The values of the ε_{4f}-E_F calculated by using Slater's transition state corresponding to the $4f$-to-$5d$ transition are tabulated in Table I, and comparison with experiments is shown in Fig. 2. The agreement between calculations and experiments is satisfactory for trivalent CeB_6, PrB_6, NdB_6, SmB_6, and GdB_6, and divalent YbB_6. For trivalent TbB_6, DyB_6, and HoB_6, there are sizable experimental energy splittings due to the $4f$ multiplets; however, if the most intense peak located on the lowest-energy side is compared with the calculated value, we can also find satisfactory agreement between calculations and experiments for these compounds. The present calculations generally predict the results of ε_{4f}-E_F for XPS on CeB_6, PrB_6, NdB_6, SmB_6, GdB_6, and YbB_6. From this and the fact that the screening of $4f$ states by $5d$ electrons plays an important role in XPS,[4-6] we can say that the Slater transition state adopted for the transition from $4f$ to $5d$ states partly includes the effect of the screening of $4f$ states by $5d$ electrons. This may be the reason for the success of the calculation for XPS on those RB_6, except for TbB_6, DyB_6, and HoB_6, which seem to have noticeable effects due to the $4f$ multiplets.

B. Comparison with BIS

In divalent YbB_6 and trivalent LuB_6, there is no vacancy in the $4f$ state which can accept an electron, so BIS measured for these compounds reflects the nature of the conduction band. Thus it is natural to consider that the spectral difference between these compounds (YbB_6 and LuB_6) and other RB_6's originates from the $4f$ states. Here it is noted that in the BIS experiment in Ref. 14, the intensity of BIS observed for YbB_6 is small compared with those for LaB_6, CeB_6, PrB_6, GdB_6, TbB_6, and DyB_6.[26] The values in eV of ε_{4f}-E_F obtained from BIS are tabulated in Table I. The charge neutrality in a sample must also be satisfied in BIS experiments like those in XPS. Therefore, for the charge neutrality to be satisfied, in the present paper we introduce the assumption that the change of the ionicity of an electron-accepted metal R^* is screened by the first-nearest-neighbor boron B whose number is 24. Now let us calculate the energy level of the $4f$ state by using Eq. (C2c). The first and third terms on the right-hand side of Eq. (C2c) are first principally evaluated by doing SCF atomic-structure calculations and using the muffin-tin potential. Thus, in the following, we describe how the Madelung term, which is the second one on the right-hand side of Eq. (C2c), suffers from the change in the BIS experiment.

If we denote the Madelung term, which is defined by the third term on the right-hand side of Eq. (B7b), as

TABLE I. Comparison of the values ε_{4f}-E_F of $4f$ levels ε_{4f} relative to Fermi levels E_F calculated for trivalent RB_6 (R=La, Ce, Pr, Nd, Sm, Gd, Tb, Dy, Ho, Er, Tm, and Lu) and divalent RB_6 (R=Sm, Eu, and Yb) with the corresponding experimental values. The ionicities of metal elements R are also shown together with the electron configurations for the R's used in the self-consistent-field (SCF) atomic-structure calculations. The value of $\Delta\varepsilon_{4f}^{(B-X)}$ is the difference between the energy eigenvalues for the $4f$ orbit of metal elements R obtained from the SCF calculations using the electron configurations of $Xe+4f^{n+0.5}5d^{0.5}$ and $Xe+4f^{n-0.5}5d^{0.5}$. These electron configurations represent Slater's transition states for the transition between $4f$ and $5d$ states which are used to understand the experimental situations of bremsstrahlung isochromat spectra (BIS) and x-ray photoemission spectroscopy (XPS). The value of $\Delta\varepsilon_{4f}^{(B-X)}$ is equal to a so-called "f-f Coulomb interaction constant U_{ff}," and this value minus the Coulomb energy $2/d_0$ evaluated from the distance d_0 between R and B is equal to the difference between the energy values of ε_{4f}-E_F obtained from $4f^{n+0.5}5d^{0.5}$ and $4f^{n-0.5}5d^{0.5}$ configurations. All the energies are in units of eV.

Crystal	Ionicity(config.):	$\varepsilon_{4f}-E_F$ cal.	expt.	$\Delta\varepsilon_{4f}^{(B-X)}$	$2/d_0$
LaB_6	$+3(4f^0 5d^0)$:	1.84			4.70
	$+2(4f^{0.5}5d^{0.5})$:	10.8	5.5[a]		
CeB_6	$+3(4f^1 5d^0)$:	0.561		17.3	4.72
	$+3(4f^{0.5}5d^{0.5})$:	−2.97	−2.5[b]		
	$+2(4f^{1.5}5d^{0.5})$:	9.58	4.0[a]		
PrB_6	$+3(4f^2 5d^0)$:	−2.22		17.5	4.74
	$+3(4f^{1.5}5d^{0.5})$:	−5.66	−5.5,[a] −4.7[b]		
	$+2(4f^{2.5}5d^{0.5})$:	7.06	4.0[a]		
NdB_6	$+3(4f^3 5d^0)$:	−1.49		17.5	4.73
	$+3(4f^{2.5}5d^{0.5})$:	−5.02	−7.0[c]		
	$+2(4f^{3.5}5d^{0.5})$:	7.78			
SmB_6	$+3(4f^5 5d^0)$:	−4.47		18.4	4.73
	$+3(4f^{4.5}5d^{0.5})$:	−8.37	−7.5,[c] −9.5[c]		
	$+2(4f^{5.5}5d^{0.5})$:	5.31			
	$+2(4f^6 5d^0)$:	5.85		15.0	4.73
	$+2(4f^{5.5}5d^{0.5})$:	2.93	−0.1,[c] −0.9,[c] −3.1[c]		
	$+1(4f^{6.5}5d^{0.5})$:	13.18			
EuB_6	$+2(4f^7 5d^0)$:	5.19		15.0	4.68
	$+2(4f^{6.5}5d^{0.5})$:	2.08			
	$+1(4f^{7.5}5d^{0.5})$:	12.4			
GdB_6	$+3(4f^7 5d^0)$:	−5.89		18.4	4.75
	$+3(4f^{6.5}5d^{0.5})$:	−9.62	−10.0[a]		
	$+2(4f^{7.5}5d^{0.5})$:	4.04	4.0[a]		
TbB_6	$+3(4f^8 5d^0)$:	−6.37		18.8	4.76
	$+3(4f^{7.5}5d^{0.5})$:	−10.1	−11.0,[a] −9.5,[a] −4.0[a]		
	$+2(4f^{8.5}5d^{0.5})$:	3.91	3.0[a]		
DyB_6	$+3(4f^9 5d^0)$:	−6.95		18.9	4.77
	$+3(4f^{8.5}5d^{0.5})$:	−10.8	−10.0,[a] −5.0[a]		
	$+2(4f^{9.5}5d^{0.5})$:	3.37	3.0[a]		
HoB_6	$+3(4f^{10}5d^0)$:	−7.51		19.1	4.77
	$+3(4f^{9.5}5d^{0.5})$:	−11.3	−9.3,[c] −6.5[c]		
	$+2(4f^{10.5}5d^{0.5})$:	3.09			
ErB_6	$+3(4f^{11}5d^0)$:	−7.79		19.2	4.76
	$+3(4f^{10.5}5d^{0.5})$:	−11.9			
	$+2(4f^{11.5}5d^{0.5})$:	2.59			
TmB_6	$+3(4f^{12}5d^0)$:	−8.66		19.4	4.75
	$+3(4f^{11.5}5d^{0.5})$:	−12.5			
	$+2(4f^{12.5}5d^{0.5})$:	2.18			
YbB_6	$+2(4f^{14}5d^0)$:	3.07			4.71
	$+2(4f^{13.5}5d^{0.5})$:	−0.273	−1.0[a]		
LuB_6	$+3(4f^{14}5d^0)$:	−9.23			4.75
	$+3(4f^{13.5}5d^{0.5})$:	−13.4			

[a]Reference 14.
[b]Reference 25.
[c]Reference 13.

$E^{(R)}_{\mathrm{Mad(BIS)}}$ and separate the summation for the $\alpha(\neq 0)$ into the first-nearest-neighbor (NN) boron atoms (1st) and the remainder, $E^{(R)}_{\mathrm{Mad(BIS)}}$ is written in atomic units as

$$E^{(R)}_{\mathrm{Mad(BIS)}} = \sum_{\alpha=\mathrm{1st\ NN}} 2\delta q'_\alpha / R_\alpha + \sum_{\alpha\neq\mathrm{1st\ NN}} 2\delta q_\alpha / R_\alpha + \sum_{\alpha=\mathrm{1st\ NN}} 2\delta q_\alpha / R_\alpha - \sum_{\alpha=\mathrm{1st\ NN}} 2\delta q_\alpha / R_\alpha \ . \tag{1a}$$

The sum of the second and third terms on the right-hand side of Eq. (1a) is the regular Madelung term which corresponds to the Madelung term under a situation in the XPS experiment. The value of charge $\delta q'_\alpha$ of borons in the first nearest neighbor is given by $\delta q_\alpha - (\frac{1}{24})$, and the value of δq_α is $\frac{1}{2}$ or $\frac{1}{3}$ for trivalent or divalent RB_6. Therefore, Eq. (1a) is simply evaluated as

$$E^{(R)}_{\mathrm{Mad(BIS)}} = E^{(R)}_{\mathrm{Mad}} - (2/d_0) \ , \tag{1b}$$

where d_0 is the distance between the R^* and the first-nearest-neighbor borons. The values of ε_{4f}-E_F obtained by using $E^{(R)}_{\mathrm{Mad(BIS)}}$ are tabulated in Table I and compared with the experimental values in Fig. 2. From Fig. 2, we can see that the values of ε_{4f}-E_F are well predicted by the calculations for GdB_6, TbB_6, and DyB_6, but they are overestimated for LaB_6, CeB_6, and PrB_6.

C. Energy difference between the most intense peaks of BIS and XPS

The energy difference $\Delta\varepsilon^{(B-X)}$ defined by $\varepsilon^{(R)}_{4f(\mathrm{BIS})} - \varepsilon^{(R)}_{4f(\mathrm{XPS})}$ is simply given by using Eq. (C2c):

$$\Delta\varepsilon^{(B-X)} = [\varepsilon^{(R)(\mathrm{SCF})}_{4f(\mathrm{BIS})} - \varepsilon^{(R)(\mathrm{SCF})}_{4f(\mathrm{XPS})}] + [E^{(R)}_{\mathrm{Mad(BIS)}} - E^{(R)}_{\mathrm{Mad(XPS)}}] + \langle \phi^{(R)}_{4f(\mathrm{BIS})} | V_{\mathrm{cry}} - V^{(R)}_{\mathrm{atom(BIS)}} | \phi^{(R)}_{4f(\mathrm{BIS})} \rangle - \langle \phi^{(R)}_{4f(\mathrm{XPS})} | V_{\mathrm{cry}} - V^{(R)}_{\mathrm{atom(XPS)}} | \phi^{(R)}_{4f(\mathrm{XPS})} \rangle \ . \tag{2a}$$

Here we have found that the absolute value of the sum of the third and fourth bracket terms on the right-hand side of Eq. (2a) is negligibly small (less than 0.05 eV) for all RB_6's. Therefore, $\Delta\varepsilon^{(B-X)}$ is given by using Eq. (1b) as follows:

$$\Delta\varepsilon^{(B-X)} = [\varepsilon^{(R)(\mathrm{SCF})}_{4f(\mathrm{BIS})} - \varepsilon^{(R)(\mathrm{SCF})}_{4f(\mathrm{XPS})}] - (2/d_0) \ , \tag{2b}$$

where the $\varepsilon^{(R)(\mathrm{SCF})}_{4f(\mathrm{BIS})}$ and $\varepsilon^{(R)(\mathrm{SCF})}_{4f(\mathrm{XPS})}$ are, respectively, the energy eigenvalues for the $4f$ orbit of the metal element R which were obtained from the SCF atomic-structure calculations using the electron configurations $\mathrm{Xe}+4f^{n+0.5}5d^{0.5}6s^0$ and $\mathrm{Xe}+4f^{n-0.5}5d^{0.5}6s^0$ $(1 \le n \le 13)$. Here we should mention that the difference between these two electron configurations is only the difference of the number of electrons in the $4f$ orbit, which is equal just to $[n+0.5-(n-0.5)]$. Therefore, the $\varepsilon^{(R)(\mathrm{SCF})}_{4f(\mathrm{BIS})} - \varepsilon^{(R)(\mathrm{SCF})}_{4f(\mathrm{XPS})}$ (hereafter we denote this as $\Delta\varepsilon^{(B-X)}_{4f}$) should coincide with a so-called "f-f Coulomb interaction constant U_{ff}." Usually, the value of the U_{ff} is estimated by using the experimental data. For example, the value of Ce is known to be about 15 eV.[27] The values for $\Delta\varepsilon^{(B-X)}_{4f}$ obtained from SCF calculations are tabulated in Table I for R^{+3} (R = Ce, Pr, Nd, Sm, Gd, Tb, Dy, Ho, Er, and Tm) and R^{+2} (R = Sm and Eu). We note that the value of 17.3 eV calculated for Ce^{+3} is satisfactory compared with about 15 eV deduced experimentally.

We have found that the energy difference $\Delta\varepsilon^{(B-X)}$ between the most intense peaks of BIS and XPS is given by the atomic term $\Delta\varepsilon^{(B-X)}_{4f}$ $(=U_{ff})$, and the difference of Madelung energies $E^{(R)}_{\mathrm{Mad(BIS)}}$ and $E^{(R)}_{\mathrm{Mad(XPS)}}$ which arises from the change of the ionicity of an electron-accepted metal in BIS, and that the values of $\Delta\varepsilon^{(B-X)}$ calculated for GdB_6, TbB_6, and DyB_6 are in good agreement with experimental ones, but those for CeB_6 and PrB_6 are not.

At the end of this section, we will briefly discuss the discrepancy between calculated ε_{4f}-E_F's and experimental results estimated from BIS for LaB_6, CeB_6, and PrB_6. We have found that values of ε_{4f}-E_F obtained from XPS for CeB_6, PrB_6, NdB_6, SmB_6, GdB_6, and YbB_6, and those from BIS for GdB_6, TbB_6, and DyB_6 are approximately predicted by our approach based on MOPW band-structure calculations and SCF atomic-structure calculations including the Slater transition state, but that for XPS for TbB_6, DyB_6, and HoB_6 there are sizable differences due to the many-electron effect. Generally speaking, there is also an effect of $4f$ multiplets in the case of BIS. Here we present the results of Herbst, Watson, and Wilkins for ε_{4f}-E_F in rare-earth metals calculated by including the effect of many electrons. For rare-earth metals, Herbst, Watson, and Wilkins performed calculations taking into account Hund's rule $4f^{n-1}$ and $4f^{n+1}$ ground levels which correspond to XPS and BIS, respectively, on the basis of relativistic Hartree-Fock calculations for atoms using a "completely screened" approximation, and the band-structure calculation by which the Fermi level E_F has been determined assuming parabolic s-band and rectangular d-band densities of states. Their results for rare-earth metals, which are tabulated in Table I in Ref. 5 as Δ_- and in Table II (Ref. 6) as Δ_+, are shown in Fig. 2. We can see from Fig. 2 that the experimental values of ε_{4f}-E_F estimated from XPS and BIS for rare-earth hexaborides are explained by their calculations for rare-earth metals. This observation indicates that the considerable difference between our calculation and the BIS experiment for LaB_6, CeB_6, and PrB_6 is due to the fact that we do not take into account the effect of the $4f$ multiplets. Therefore, we can say at least that XPS for CeB_6, PrB_6, NdB_6, SmB_6, GdB_6, and YbB_6, and BIS for GdB_6, TbB_6, and DyB_6, shows that the effect of $4f$ multiplets is small compared to that in XPS for TbB_6, DyB_6, and HoB_6 and BIS for LaB_6, CeB_6, and

PrB_6. This would be the reason why our calculations based on the one-electron approximation are approximately applicable to XPS for CeB_6, PrB_6, NdB_6, SmB_6, GdB_6, and YbB_6, and BIS for GdB_6, TbB_6, and DyB_6.

IV. SUMMARY

We have calculated the electronic structures of trivalent rare-earth hexaborides RB_6 (R = La, Ce, Pr, Nd, Sm, Gd, Tb, Dy, Ho, Er, Tm, and Lu) and divalent RB_6 ones (R = Sm, Eu, and Yb) by using the modified orthogonalized-plane-wave (MOPW) method within the framework of the muffin-tin (MT) potential approximation based on the self-consistent-field (SCF) atomic-structure calculation. It has been found that the densities of states obtained are almost the same for the different RB_6's with the same valency, except for the energy position of the pointed density of states originated from the $4f$ states.

In order to take into account as accurately as possible the experimental situations of x-ray photoemission spectroscopy (XPS) and bremsstrahlung isochromat spectra (BIS) for RB_6, the concept of the transition state introduced by Slater has been adopted for the transition between $4f$ and $5d$ states. By using Slater's transition state, which includes the effect of the screening of $4f$ states by $5d$ electrons, it has been shown that SCF atomic-structure calculations using electron configurations representing Slater's transition states provide values of a so-called "f-f Coulomb interaction constant U_{ff}," and that its value for Ce^{+3} is satisfactory compared to the value estimated experimentally. Furthermore, we have found that the values ε_{4f}-E_F of the $4f$ levels ε_{4f} relative to the Fermi level E_F calculated using Slater's transition state approximately predict experimental values obtained from XPS for trivalent CeB_6, PrB_6, NdB_6, SmB_6, GdB_6, and divalent YbB_6, and BIS for trivalent GdB_6, TbB_6, and DyB_6. However, it has been shown that there is a considerable difference between calculation and experiment for XPS for TbB_6, DyB_6, and HoB_6, and BIS for LaB_6, CeB_6, and PrB_6. Its origin is mainly attributed to the effect of $4f$ multiplets, which is not taken into account in the present calculation.

ACKNOWLEDGMENTS

The author would like to thank Professor S. Suga, Osaka University, and Professor S. Muramatsu, Utsunomiya University, for their valuable comments.

APPENDIX A: MOPW METHOD

In the MOPW method,[18] the wave function $\Psi_{\mathbf{k}}(\mathbf{r})$ is represented by the linear combination of the wave functions of the OPW and tight-binding methods. The Schrödinger equation to be solved is

$$H\Psi_{\mathbf{k}}(\mathbf{r})=\lambda_{\mathbf{k}}\Psi_{\mathbf{k}}(\mathbf{r}) , \tag{A1}$$

where H is a Hamiltonian consisting of a kinetic-energy term and the crystal potential $V_{\rm cry}(\mathbf{r})$, which is periodic with the periodicity of the lattice. The wave function $\Psi_{\mathbf{k}}(\mathbf{r})$ specified by a wave vector $\mathbf{k}$ within the first Brillouin zone (BZ) is written as follows:

$$\Psi_{\mathbf{k}}(\mathbf{r})=\sum_{\mathbf{G}} c(\mathbf{k}+\mathbf{G})\psi_{\mathbf{k}+\mathbf{G}}(\mathbf{r})+\sum_{\xi}\sum_{Lv} u_{Lv}^{(\xi)}(\mathbf{k})\chi_{Lv}^{(\xi)}(\mathbf{k},\mathbf{r}) . \tag{A2a}$$

Here, $\mathbf{G}$ is a reciprocal-lattice vector, and the function $\psi_{\mathbf{k}+\mathbf{G}}(\mathbf{r})$ is the orthogonalized plane wave given as follows:

$$\begin{aligned}\psi_{\mathbf{k}+\mathbf{G}}(\mathbf{r})&=e^{i(\mathbf{k}+\mathbf{G})\cdot\mathbf{r}}/\sqrt{V}\\&\quad-\sum_{\mu}\sum_{Lc} v_{Lc}^{(\mu)}(\mathbf{k}+\mathbf{G})\chi_{Lc}^{(\mu)}(\mathbf{k}+\mathbf{G},\mathbf{r}) ,\\&\equiv|\mathbf{k}+\mathbf{G}\rangle-\sum_{\mu}\sum_{Lc} v_{Lc}^{(\mu)}(\mathbf{k}+\mathbf{G})|\chi_{Lc}^{(\mu)}(\mathbf{k}+\mathbf{G},\mathbf{r})\rangle ,\end{aligned} \tag{A2b}$$

where V is the volume of a crystal. In Eqs. (A2a) and (A2b), suffixes ξ and μ mean that the independent site and the functions $\chi_{Lv}^{(\xi)}(\mathbf{k},\mathbf{r})$ and $\chi_{Lc}^{(\mu)}(\mathbf{k}+\mathbf{G},\mathbf{r})$ are Bloch functions characterized by the collective indexes $Lv=(l_v,m_v)$ and $Lc=(l_c,m_c)$ for the quantum states of valence and core orbitals. For example, the Bloch function $|\chi_{Lc}^{(\mu)}(\mathbf{k}+\mathbf{G},\mathbf{r})\rangle$ is given as follows:

$$|\chi_{Lc}^{(\mu)}(\mathbf{k}+\mathbf{G},\mathbf{r})\rangle=\sum_{\mathbf{R}_t} e^{i(\mathbf{k}+\mathbf{G})\cdot(\mathbf{R}_t+\mathbf{d}_\mu)}|\phi_{Lc}^{(\mu)}(\mathbf{r}-\mathbf{R}_t-\mathbf{d}_\mu)\rangle/\sqrt{N_\mu} . \tag{A2c}$$

Here N_μ is the number of the μ atom, $\mathbf{R}_t$ is the translation vector written by using primitive vectors τ_1, τ_2, and τ_3 as $l\tau_1+m\tau_2+n\tau_3$ with integers l, m, and n, and the function $|\phi_{Lc}^{(\mu)}(\mathbf{r}-\mathbf{R}_t-\mathbf{d}_\mu)\rangle$ is the atomic core orbital with the quantum state L_c for the μ atom located at $\mathbf{R}_t+\mathbf{d}_\mu$, where $\mathbf{d}_\mu$ is the position vector of the μ atom in a unit cell measured from the origin for the unit cell.

The orthogonality between the Bloch function $|\chi_{Lc'}^{(\nu)}(\mathbf{k}+\mathbf{G},\mathbf{r})\rangle$ constructed from the core orbital $\phi_{Lc'}^{(\nu)}(\mathbf{r})$ of the ν atom and the orthogonalized plane wave $|\psi_{\mathbf{k}+\mathbf{G}}(\mathbf{r})\rangle$ leads to the following form for $|\psi_{\mathbf{k}+\mathbf{G}}(\mathbf{r})\rangle$:

$$|\psi_{\mathbf{k}+\mathbf{G}}(\mathbf{r})\rangle=|\mathbf{k}+\mathbf{G}\rangle-\sum_{\mu}\sum_{Lc}|\chi_{Lc}^{(\mu)}(\mathbf{k}+\mathbf{G},\mathbf{r})\rangle\times\langle\chi_{Lc}^{(\mu)}(\mathbf{k}+\mathbf{G},\mathbf{r})|\mathbf{k}+\mathbf{G}\rangle . \tag{A3}$$

By inserting the wave function $\Psi_{\mathbf{k}}(\mathbf{r})$ obtained from Eqs. (A2) and (A3) into Eq. (A1), the following secular equation is derived:

$$\mathbf{H}(\mathbf{k})\boldsymbol{\omega}(\mathbf{k})=\lambda_{\mathbf{k}}\boldsymbol{\Delta}(\mathbf{k})\boldsymbol{\omega}(\mathbf{k}) . \tag{A4a}$$

Here, $\boldsymbol{\omega}(\mathbf{k})$ is a vector such as $\boldsymbol{\omega}(\mathbf{k})=\{\ldots,c(\mathbf{k}+\mathbf{G}),\ldots,u_{Lv}^{(\xi)}(\mathbf{k}),\ldots\}^{\tau}$, and the matrices $\mathbf{H}(\mathbf{k})$ and $\boldsymbol{\Delta}(\mathbf{k})$ consist of matrices $\mathbf{H}_{\mathbf{G}',\mathbf{G}}(\mathbf{k})$, $\boldsymbol{\Delta}_{\mathbf{G}',\mathbf{G}}(\mathbf{k})$, $\mathbf{H}_{\mathbf{G}',Lv}^{(\xi)}(\mathbf{k})$, $\boldsymbol{\Delta}_{\mathbf{G}',Lv}^{(\xi)}(\mathbf{k})$, $\mathbf{H}_{Lv',Lv}^{(\xi')(\xi)}(\mathbf{k})$, and $\boldsymbol{\Delta}_{Lv',Lv}^{(\xi')(\xi)}(\mathbf{k})$ as shown below:

$$\mathbf{H}(\mathbf{k})=\begin{vmatrix} \mathbf{H}_{\mathbf{G}',\mathbf{G}}(\mathbf{k}) & \mathbf{H}^{(\xi)}_{\mathbf{G}',Lv}(\mathbf{k}) \\ \mathbf{H}^{(\xi)}_{\mathbf{G}',Lv}(\mathbf{k})^* & \mathbf{H}^{(\xi')(\xi)}_{Lv',Lv}(\mathbf{k}) \end{vmatrix} , \tag{A4b}$$

$$\mathbf{\Delta}(\mathbf{k})=\begin{vmatrix} \Delta_{\mathbf{G}',\mathbf{G}}(\mathbf{k}) & \Delta^{(\xi)}_{\mathbf{G}',Lv}(\mathbf{k}) \\ \Delta^{(\xi)}_{\mathbf{G}',Lv}(\mathbf{k})^* & \Delta^{(\xi')(\xi)}_{Lv',Lv}(\mathbf{k}) \end{vmatrix} . \tag{A4c}$$

The matrix elements $H_{\mathbf{G}',\mathbf{G}}(\mathbf{k})$ and $\Delta_{\mathbf{G}',\mathbf{G}}(\mathbf{k})$ are given as

$$H_{\mathbf{G}',\mathbf{G}}(\mathbf{k})=(\mathbf{k}+\mathbf{G})^2\delta_{\mathbf{G},\mathbf{G}'}+\langle \mathbf{G}'|V_{\rm cry}(\mathbf{r})|\mathbf{G}\rangle - \sum_{\mu}\sum_{Lc}\varepsilon^{(\mu)}_{Lc}\langle \mathbf{k}+\mathbf{G}'|\chi^{(\mu)}_{Lc}(\mathbf{k}+\mathbf{G},\mathbf{r})\rangle \times\langle \chi^{(\mu)}_{Lc}(\mathbf{k}+\mathbf{G},\mathbf{r})|\mathbf{k}+\mathbf{G}\rangle \tag{A5a}$$

and

$$\Delta_{\mathbf{G}',\mathbf{G}}(\mathbf{k})=\delta_{\mathbf{G},\mathbf{G}'}-\sum_{\mu}\sum_{Lc}\langle \mathbf{k}+\mathbf{G}'|\chi^{(\mu)}_{Lc}(\mathbf{k}+\mathbf{G},\mathbf{r})\rangle \times\langle \chi^{(\mu)}_{Lc}(\mathbf{k}+\mathbf{G},\mathbf{r})+\mathbf{k}+\mathbf{G}\rangle , \tag{A5b}$$

where $\varepsilon^{(\mu)}_{Lc}$ is the energy eigenvalue of the Lc state of the μ atom (the detail of $\varepsilon^{(\mu)}_{Lc}$ is given in Appendix C), and the bracket term is given by

$$\langle \mathbf{k}+\mathbf{G}'|\chi^{(\mu)}_{Lc}(\mathbf{k}+\mathbf{G},\mathbf{r})\rangle\langle \chi^{(\mu)}_{Lc}(\mathbf{k}+\mathbf{G},\mathbf{r})|\mathbf{k}+\mathbf{G}\rangle =(4\pi N_\mu/V)e^{i\mathbf{q}\cdot\mathbf{d}_\mu}(2l_c+1)P_{lc}(\cos\theta)\int_0^\infty r^2 j_{lc}(|\mathbf{k}+\mathbf{G}|r)R^{(\mu)}_{nclc}(r)dr\int_0^\infty r^2 j_{lc}(|\mathbf{k}+\mathbf{G}'|r)R^{(\mu)}_{nclc}(r)dr . \tag{A5c}$$

Here, vector $\mathbf{q}=\mathbf{G}-\mathbf{G}'$, and θ is the angle between vectors $\mathbf{k}+\mathbf{G}$ and $\mathbf{k}+\mathbf{G}'$. $P_{lc}(z)$ and $j_{lc}(|\mathbf{k}+\mathbf{G}|r)$ are Legendre and spherical Bessel functions of the lcth, respectively, and $R^{(\mu)}_{nclc}(r)$ is the radial wave function of the atomic orbital $\phi^{(\mu)}_{Lc}(r)$, which is obtained from self-consistent-field (SCF) atomic-structure calculations based on the prescription of Herman and Skillman.[16] $\langle \mathbf{G}'|V_{\rm cry}(\mathbf{r})|\mathbf{G}\rangle$ is the Fourier component of the crystal potential $V_{\rm cry}(\mathbf{r})$, and is described in Appendix B.

The matrix elements $H^{(\xi)}_{\mathbf{G}',Lv}(\mathbf{k})$ and $\Delta^{(\xi)}_{\mathbf{G}',Lv}(\mathbf{k})$ are given by

$$H^{(\xi)}_{\mathbf{G}',Lv}(\mathbf{k})=(\mathbf{k}+\mathbf{G}')^2\Delta^{(\xi)}_{\mathbf{G}',Lv}(\mathbf{k}) +\langle \mathbf{k}+\mathbf{G}'|V_{\rm cry}(\mathbf{r})|\chi^{(\xi)}_{Lv}(\mathbf{k},\mathbf{r})\rangle , \tag{A6a}$$

$$\Delta^{(\xi)}_{\mathbf{G}',Lv}(\mathbf{k})=(N_\xi/V)^{1/2}e^{-i\mathbf{G}'\cdot\mathbf{d}_\xi}4\pi(-i)^{l_v}Y_{Lv}(\mathbf{k}+\mathbf{G}') \times\int_0^\infty r^2 j_{lv}(|\mathbf{k}+\mathbf{G}'|r)R^{(\xi)}_{nvlv}(r)dr , \tag{A6b}$$

and the matrix elements $H^{(\xi')(\xi)}_{Lv',Lv}(\mathbf{k})$ and $\Delta^{(\xi')(\xi)}_{Lv',Lv}(\mathbf{k})$ are given as follows:

$$H^{(\xi')(\xi)}_{Lv',Lv}(\mathbf{k})=\sum_{\mathbf{R}_\xi}e^{i\mathbf{k}\cdot\mathbf{R}_\xi}\langle \phi^{(\xi')}_{lv'}(\mathbf{r})|H|\phi^{(\xi)}_{Lv}(\mathbf{r}-\mathbf{R}_\xi)\rangle , \tag{A6c}$$

$$\Delta^{(\xi')(\xi)}_{Lv',Lv}(\mathbf{k})=\sum_{\mathbf{R}_\xi}e^{i\mathbf{k}\cdot\mathbf{R}_\xi}\langle \phi^{(\xi')}_{Lv'}(\mathbf{r})|\phi^{(\xi)}_{Lv}(\mathbf{r}-\mathbf{R}_\xi)\rangle , \tag{A6d}$$

where a function $Y_{Lv}(\mathbf{k}+\mathbf{G}')$ in Eq. (A6b) is an example of spherical harmonics in a real form. The method for evaluating the matrix elements or overlap integral in Eqs. (A6a), (A6c), and (A6d) will be described in Appendix C.

APPENDIX B: FOURIER COMPONENT OF THE CRYSTAL POTENTIAL

For the evaluation of the Fourier component $\langle \mathbf{G}'|V_{\rm cry}(\mathbf{r})|\mathbf{G}\rangle$ of crystal potential $V_{\rm cry}(\mathbf{r})$, there are two methods. One uses the crystal potential represented by the linear combination of the atomiclike potential (LCAP), and other is that using the muffin-tin (MT) potential. In this appendix, we first describe the former method and point out that it is not appropriate for a calculation of the energy-band structure of a crystal in which the effect of charge transfer must be taken into account exactly. Next, we describe the latter method based on the MT potential, and show that it is applicable not only to the case where the effect of charge transfer is not important, but also to the case where the effect of charge transfer must be considered.

1. Fourier component of crystal potential using the LCAP method

The crystal potential $V_{\rm cry}(\mathbf{r})$ is given by[23]

$$V_{\rm cry}(\mathbf{r})=V_c(\mathbf{r})+V_x(\mathbf{r}) , \tag{B1a}$$

where $V_c(\mathbf{r})$ and $V_x(\mathbf{r})$ are Coulombic and exchange parts of the crystal potential, respectively, and given as follows:

$$V_c(\mathbf{r})=\sum_{\mathbf{R}_t}\sum_{\mu}V^{(\rm at)}_\mu(\mathbf{r}-\mathbf{R}_t-\mathbf{d}_\mu) , \tag{B1b}$$

$$V_x(\mathbf{r})=-6\alpha_{\rm ex}\{3\rho(\mathbf{r})/8\pi\}^{1/3} , \tag{B1c}$$

$$\rho(\mathbf{r})=\sum_{\mathbf{R}_t}\sum_{\mu}\rho^{(\rm at)}_\mu(\mathbf{r}-\mathbf{R}_t-\mathbf{d}_\mu) . \tag{B1d}$$

Here, $\alpha_{\rm ex}$ is the exchange parameter, having a value of 0.7 for rare-earth elements and 0.764 52 for boron;[28] $V^{(\rm at)}_\mu(\mathbf{r}-\mathbf{R}_t-\mathbf{d}_\mu)$ and $\rho^{(\rm at)}_\mu(\mathbf{r}-\mathbf{R}_t-\mathbf{d}_\mu)$, respectively, are the atomic Coulomb potential and the atomic electron density of the μ atom located at $\mathbf{R}_t+\mathbf{d}_\mu$. If the exchange parts of the crystal potential, $V_x(\mathbf{r})$, are written as

$$V_x(\mathbf{r})=-6\alpha_{\rm ex}\left\{3\sum_{\mathbf{R}_t}\sum_{\mu}\rho^{(\rm at)}_\mu(\mathbf{r}-\mathbf{R}_t-\mathbf{d}_\mu)/8\pi\right\}^{1/3} =\sum_{\mathbf{R}_t}\sum_{\mu}(-6)\zeta_\mu(\mathbf{r})\alpha_{\rm ex}\{3\rho^{(\rm at)}_\mu(\mathbf{r})/8\pi\}^{1/3} =\sum_{\mathbf{R}_t}\sum_{\mu}z^{(\rm at)}_\mu(\mathbf{r}-\mathbf{R}_t-\mathbf{d}_\mu) , \tag{B2}$$

the crystal potential $V_{\rm cry}(\mathbf{r})$ is represented by the linear combination of atomiclike potential $Z_\mu^{(\rm at)}(r)$ defined by the following equation:

$$V_{\rm cry}(\mathbf{r})=\sum_{\mathbf{R}_t}\sum_{\mu}\{V_\mu^{(\rm at)}(\mathbf{r}-\mathbf{R}_t-\mathbf{d}_\mu)+z_\mu^{(\rm at)}(\mathbf{r}-\mathbf{R}_t-\mathbf{d}_\mu)\}=\sum_{\mathbf{R}_t}\sum_{\mu}Z_\mu^{(\rm at)}(\mathbf{r}-\mathbf{R}_t-\mathbf{d}_\mu)\ . \tag{B3}$$

By using Eq. (B3), the Fourier component $\langle\mathbf{G}'|V_{\rm cry}(\mathbf{r})|\mathbf{G}\rangle$ of the crystal potential is given as

$$\langle\mathbf{G}'|V_{\rm cry}(\mathbf{r})|\mathbf{G}\rangle=\sum_{\mu}(N_\mu/V)e^{i\mathbf{q}\cdot\mathbf{d}_\mu}\int_0^\infty 4\pi r^2 j_0(qr)Z_\mu^{(\rm at)}(r)dr\ . \tag{B4}$$

In order to calculate Eq. (B4), we have to evaluate the value of the atomiclike potential $Z_\mu^{(\rm at)}(r)$. It is very troublesome to obtain the value of $\zeta_\mu(\mathbf{r})$ defined by Eq. (B2), and furthermore, if we consider the case in which the effect of the charge transfer must be taken into account, the potential $Z_\mu^{(\rm at)}(r)$ becomes a long-ranged form due to the existence of the long-ranged Coulomb potential. Here it should be noted that the potential $Z_\mu^{(\rm at)}(r)$ is a short-ranged type when the atom is neutral. This fact means that it is troublesome to calculate the Fourier component of the crystal potential by using Eq. (B4), when the effect of the charge transfer must be taken into account.

2. Fourier component of crystal potential using the muffin-tin approximation

The Fourier component term $\langle\mathbf{G}'|V_{\rm cry}(r)|\mathbf{G}\rangle$ is given by

$$\langle\mathbf{G}'|V_{\rm cry}(\mathbf{r})|\mathbf{G}\rangle=V^{-1}\int_V e^{i\mathbf{q}\cdot\mathbf{r}}V_{\rm cry}(\mathbf{r})d\mathbf{r}\ . \tag{B5}$$

If we divide the volume V of a crystal into atom cells whose volume is Ω_μ, the following relation holds:

$$\int_V d\mathbf{r}=\sum_{\mathbf{R}_t}\sum_{\mu}\int_{\Omega_\mu}d\mathbf{r}\ .$$

Moreover, if we choose the muffin-tin (MT) zero as the origin of energy for the integrations, the volume Ω_μ is reduced to the volume $\Omega_\mu^{(0)}$ of the MT sphere. Therefore, Eq. (B5) is rewritten using the MT potential $V_{\rm MT}^{(\mu)}(r)$ measured from the MT zero as follows:

$$\langle\mathbf{G}'|V_{\rm cry}(\mathbf{r})|\mathbf{G}\rangle=\sum_{\mu}(N_\mu/V)e^{i\mathbf{q}\cdot\mathbf{d}_\mu}\int_{\Omega_\mu^{(0)}}e^{i\mathbf{q}\cdot\mathbf{r}}V_{\rm MT}^{(\mu)}(r)d\mathbf{r}=\sum_{\mu}(N_\mu/V)e^{i\mathbf{q}\cdot\mathbf{d}_\mu}\int_0^{R_{\rm MT}^{(\mu)}}4\pi r^2 j_0(qr)V_{\rm MT}^{(\mu)}(r)dr\ , \tag{B6}$$

where the MT radius $R_{\rm MT}^{(\mu)}$ is defined by $\{3\Omega_\mu^{(0)}/4\pi\}^{1/3}$.

Theoretical details for the construction of the MT potential have already been described in our previous paper,[23] in which we studied the x-ray-absorption near-edge structure (XANES) of ionic crystals by using a multiple-scattering theory based on the muffin-tin potential approximation. In the present paper, therefore, we present only the final form for the MT potential.

If we denote an atom that we consider to be the origin of space by the index $\alpha=0$, and specify atoms surrounding it by $\alpha(\neq 0)$, the MT potential $V_{\rm MT}(r)$ is given as

$$V_{\rm MT}(r)=V_c^{(s)}(r)-6\alpha_{\rm ex}\{3\rho^{(s)}(r)/8\pi\}^{1/3}\ , \tag{B7a}$$

$$V_c^{(s)}(r)=V_c^{(\rm at)}(r)+(2r)^{-1}\sum_{\alpha\neq 0}R_\alpha^{-1}\int_{R_\alpha-r}^{R_\alpha+r}r_\alpha W(r_\alpha)dr_\alpha+\sum_{\alpha\neq 0}2\delta q_\alpha/R_\alpha\ , \tag{B7b}$$

$$\rho^{(s)}(r)=\rho^{(\rm at)}(r)+(2r)^{-1}\sum_{\alpha\neq 0}R_\alpha^{-1}\int_{R_\alpha-r}^{R_\alpha+r}r_\alpha\rho^{(\rm at)}(r_\alpha)dr_\alpha\ . \tag{B7c}$$

Here, the third term on the right-hand side of Eq. (B7b) is just a Madulung term. $W(r_\alpha)$ is a short-range function introduced to separate a long-range Coulomb part due to the charge transfer, and is defined by using the value of the charge transfer δq_α as $W(r_\alpha)=V_c^{(\rm at)}(r)-2\delta q_\alpha/r_\alpha$. Here it is noted that the value of δq_α is defined by $\sum_{n\lambda}\omega_{n\lambda}^{(\alpha)}-Z_\alpha$, where Z_α and $\omega_{n\lambda}^{(\alpha)}$ are the atomic number of the αth atom and the occupation number for the orbital specified by $n\lambda$, respectively.

APPENDIX C: EVALUATION OF EQUATION (A6)

By using the muffin-tin potential, the term $\langle\mathbf{k}+\mathbf{G}'|V_{\rm cry}(\mathbf{r})|\chi_{Lv}^{(\xi)}(\mathbf{k},\mathbf{r})\rangle$ in Eq. (A6a) is evaluated as follows:

$$\langle\mathbf{k}+\mathbf{G}'|V_{\rm cry}(\mathbf{r})|\chi_{Lv}^{(\xi)}(\mathbf{k},\mathbf{r})\rangle=(N_\xi/V)^{1/2}e^{-i\mathbf{G}'\cdot\mathbf{d}_\xi}4\pi(-i)^{l_v}Y_{Lv}(\mathbf{k}+\mathbf{G}')\int_0^{R_{\rm MT}^{(\xi)}}r^2 j_{l_v}(|\mathbf{k}+\mathbf{G}'|r)V_{\rm MT}^{(\xi)}(r)R_{nvl_v}^{(\xi)}(r)dr\ . \tag{C1}$$

The method for evaluating Eqs. (A6c) and (A6d) is basically the same as in the extended Hückle tight-binding (XHTB) method.[29] In the present paper, we choose a $4f$ orbital of rare-earth elements as the basis state of the MOPW band-structure calculations; namely, $\xi=\xi'=R$ (rare-earth element) and $L_v=L_{v'}=4f$. In this case, for the most closed rare-earth atom pair, the absolute values of overlap integrals between two $4f$ orbitals (whose distance is a_0) are, for example, 4.632×10^{-5}, 9.993×10^{-6}, 7.560×10^{-7}, and 1.942×10^{-8} for σ, π, δ, and ϕ states of $4f$ orbitals of the Sm^{+3}-Sm^{+3} pair, respectively. This result means that the $4f$ orbital is strongly localized within the MT sphere, since the MT sphere $R_{\rm MT}^{(R)}$ of rare-earth element R is $a_0/2$ (see Sec. II). Therefore, Eqs. (A6c) and (A6d) are evaluated as follows:

$$H_{Lv',Lv}^{(\xi')(\xi)}(\mathbf{k})=\varepsilon_{Lv}^{(R)}\delta_{Lv',Lv}=\varepsilon_{4f}^{(R)}\delta_{mv',mv}\ , \tag{C2a}$$

$$\Delta_{Lv',Lv}^{(\xi')(\xi)}(\mathbf{k})=\delta_{Lv',Lv}=\delta_{mv',mv}\ , \tag{C2b}$$

where m_v and $m_{v'}$ are the magnetic quantum numbers in a real base. $\varepsilon_{4f}^{(R)}$ is the energy level of the $4f$ state of the rare-earth element R, and is calculated as follows:

$$\varepsilon_{4f}^{(R)}=\varepsilon_{4f}^{(R)(\rm SCF)}+E_{\rm Mad}^{(R)} +\langle\phi_{4f}^{(R)}(\mathbf{r})|V_{\rm cry}(\mathbf{r})-V_{\rm atom}^{(R)}(\mathbf{r})|\phi_{4f}^{(R)}(\mathbf{r})\rangle\ . \tag{C2c}$$

Here, $\varepsilon_{4f}^{(R)(\rm SCF)}$ is the energy eigenvalue obtained from the SCF calculation and $E_{\rm Mad}^{(R)}$ is the Madelung energy defined by the third term on the right-hand side of Eq. (B7b). Since the $4f$ state is strongly localized within the MT sphere, as already mentioned, the bracket term of Eq. (C2c) can be evaluated using the MT potential:

$$\langle\phi_{4f}^{(R)}|V_{\rm cry}-V_{\rm atom}^{(R)}|\phi_{4f}^{(R)}\rangle =\int_0^{R_{\rm MT}^{(R)}}R_{4f}^2(r)\{V_{\rm MT}^{(R)}(r)-V_{\rm atom}^{(R)}(r)\}r^2dr\ . \tag{C2d}$$

It is clear that the energy correction based on Eq. (C2d) is also useful for core states which are also localized within the MT sphere.

[1] J. W. Allan, L. I. Johansson, I. Lindau, and S. B. Hagstrom, Phys. Rev. B **21**, 1335 (1980).
[2] K. Samwer and K. Winger, Z. Phys. B **25**, 269 (1976).
[3] F. Steglich, in *Theory of Heavy Fermions and Valence Fluctuations,* edited by T. Kasuya and T. Saso (Springer-Verlag, Berlin, 1985).
[4] J. F. Herbst, D. N. Lowy, and R. E. Watson, Phys. Rev. B **6**, 1913 (1972).
[5] J. F. Herbst, R. E. Watson, and J. W. Wilkins, Phys. Rev. B **13**, 1439 (1976).
[6] J. F. Herbst, R. E. Watson, and J. W. Wilkins, Phys. Rev. B **17**, 3089 (1978).
[7] P. F. Walch, D. E. Ellis, and F. M. Mueller, Phys. Rev. B **15**, 1859 (1977).
[8] A. Hasegawa and A. Yanase, J. Phys. F **2**, 1245 (1977).
[9] H. Harima, O. Sakai, T. Kasuya, and A. Yanase, Solid State Commun. **66**, 603 (1988).
[10] Y. Kubo and S. Asano, Phys. Rev. B **39**, 8822 (1989).
[11] B. I. Min and Y. R. Jang, Phys. Rev. B **44**, 13 270 (1991).
[12] Y. Kubo, S. Asano, H. Harima, and A. Yanese, J. Phys. Soc. Jpn. **62**, 205 (1993).
[13] M. Campagna, G. K. Wertheim, and Y. Baer, in *Photoemission in Solids II,* edited by L. Ley and M. Cardona (Springer-Verlag, Berlin, 1979).
[14] Y. Mori, N. Shino, S. Imada, S. Suga, T. Nanba, M. Tomikawa, and S. Kunii, Physica B **186-188**, 66 (1993).
[15] J. C. Slater, *The Calculation of Molecular Orbitals* (Wiley, New York, 1979).
[16] F. Herman and S. Skillman, *Atomic Structure Calculations* (Prentice-Hall, Englewood Cliffs, NJ, 1963).
[17] R. W. G. Wyckoff, *Crystal Structures* (Interscience, New York, 1960), Vol. 2.
[18] R. A. Deegan and W. D. Twose, Phys. Rev. **164**, 993 (1967).
[19] C. Herring, Phys. Rev. **57**, 1169 (1940).
[20] O. V. Farberovich, S. I. Kurganskii, and E. P. Domashevskaya, Phys. Status Solidi B **94**, 51 (1979).
[21] O. V. Farberovich, S. I. Kurganskii, and E. P. Domashevskaya, Phys. Status Solidi B **97**, 631 (1980).
[22] S. I. Kurganskii and O. V. Farberovich, Phys. Status Solidi B **106**, 437 (1981).
[23] M. Kitamura, S. Muramatsu, and C. Sugiura, Phys. Status Solidi B **142**, 191 (1987).
[24] H. M. Evjen, Phys. Rev. **39**, 675 (1932).
[25] H. Sugawara, S. Kakizaki, I. Nagakura, T. Ishii, T. Komatsubara, and T. Kasuya, J. Phys. Soc. Jpn. **51**, 915 (1982).
[26] S. Suga (private communication).
[27] M. Takeshige, O. Sakai, and T. Kasuya, J. Phys. Soc. Jpn. **60**, 666 (1991).
[28] K. Schwarz, Phys. Rev. B **5**, 2466 (1972).
[29] M. Kitamura and S. Muramatsu, Phys. Rev. B **41**, 1158 (1990).